Formation and post-formation dynamics of bacterial biofilm streamers as highly viscous liquid jets (Supplementary information)

Siddhartha Das and Aloke Kumar

Department of Mechanical Engineering,

University of Alberta, Edmonton, Alberta, Canada T6G 2G8

(Dated: September 14, 2014)

In this Supplementary Information, we provide detailed discussions and derivation of different issues described in the main text.

I. RELAXATION TIME OF THE BIOFILMS

Before pinpointing the rheological parameters that are needed to characterize the biofilms, it is essential to understand the rheological response of the biofilms to external mechanical stresses. Through a volume of studies [1–4], it has been well established that the biofilms behave as viscoelastic liquids i.e., they exhibit an elastic solid-like behaviour at time t such that $t \ll \tau_{ve}$ and a liquid-like behaviour at time t such that $t \gg \tau_{ve}$. Here τ_{ve} is the viscoelastic relaxation time (or often called as the elastic relaxation time [2]) that characterizes the biofilm rheology. We shall provide more discussions on the significance of τ_{ve} later. This elastic solid-like behaviour (at $t \ll \tau_{ve}$) is characterized by the shear modulus G, whereas this liquid-like behavior (at $t \gg \tau_{ve}$) is characterized by the liquid viscosity μ_b. The viscoelastic time scale τ_{ve} is the ratio of these two parameters, i.e., $\tau_{ve} = \mu_b/G$. In short, these three parameters, namely G, μ_b and τ_{ve} dictate the rheology of the viscoelastic biofilms.

The parallel plate rheometer creep test has been the technique that has been commonly used to measure the rheological properties of any material. In this technique the concerned material is placed between the parallel rheometer plates. A constant torque is applied for a given time interval ($t \in [0, T]$), and the resulting displacement of the rheometer plate is obtained and is subsequently translated into the corresponding material strain. As long as the applied torque is sufficiently small, the material exhibits linear response, and one can witness any of the following three behaviours. First, if the material is an ideal elastic solid, it responds instantaneously to the applied stress (exerted at $t = 0$) by an instantaneous strain. This strain remains constant till the time when the stress is removed at $t = T$, and at that point of time the material recoils to its original configuration. The central material parameter for this case is the shear modulus G, which is obtained from the strain amplitude between $t = 0$ and $t = T$. Second, if the material is an ideal viscous liquid, the material exhibits a linear strain in the time period ($t \in [0, T]$) in which the stress is applied. Once the stress is removed (at $t = T$), there is no further displacement, and the material does not recoil to its original conformation. The central material parameter for this case is the liquid viscosity μ_b, which is obtained from the slope of the strain curve. Third, if the material is an idealized viscoelastic liquid it exhibits a behaviour which is a combination of the behaviours of the elastic solid and the viscous liquid. The applied torque results in an instantaneous elastic solid-like deformation (with the corresponding shear modulus G); however, over time,

the material will creep irreversibly like a viscous liquid (with a viscosity μ_b). Once the torque is withdrawn at $t = T$, there is only a partial recoil. The viscoelastic or elastic relaxation time τ_{ve} is the time needed for the irreversible deformation to completely account for the initial reversible deformation [2]. In other words, τ_{ve} can be estimated as the time needed for the viscous creep length to become equal to the elastic deformation length, which ensures that the memory of the initial condition is lost, and accordingly, we get $\tau_{ve} = \mu_b/G$.

Central to our present analysis is the knowledge about the rheological parameters (G, μ_b and τ_{ve}) of the biofilms that degenerate into streamers in presence of low Reynolds number transport. There have been massive volume of investigations that have studied these rheological parameters of biofilms – most of these studies have employed the parallel plate rheometer creep tests to obtain these rheological parameters. The most relevant of these studies, in context to our present work, is the work by Shaw et al. [2], where the authors demonstrate that the viscoelastic relaxation times (Shaw et al. [2] call it elastic relaxation time) of a wide range of biofilm samples (obtained from different sources) remain approximately the same at about 18 minutes. Shaw et al. [2] argued that there is a unique survival significance of this convergent viscoelastic behavior of the biofilms, characterized by this unique viscoelastic or elastic relaxation time of 18 minutes – this time signifies the shortest period over which the biofilms can exhibit a phenotypic response to the applied mechanical stress. This remarkable study by Shaw et al. [2] was based on the experimental results of G and μ_b values of as many as 44 different biofilms. Shaw et al. [2] themselves conducted experiments on different biofilms such as those produced by *Streptococcus mutans*, different strains of *Pseudomonas aeruginosa*, a cyanobacterial biofilm and an algal biofilm. In addition, they included data from previous experiments on biofilms [5] grown from pond water inoculum. Shaw et al. [2] reported a massive variation in G and μ_b values with the variation in the biofilms (extent of this variation was as large as seven orders of magnitude); but most remarkably the ratio μ_b/G, which is the elastic or the viscoelastic relaxation time, was invariably close to the value of 18 minutes. It is worthwhile to mention here that Shaw et al. [2] demonstrated that the possible heterogeneities intrinsic to a natural biofilm will affect μ_b and G almost equally, and accordingly the ratio μ_b/G remains unaffected. There has been a host of studies [4, 6–11] that have based their analysis on this universal value of the biofilm relaxation time, without conducting separate experiments on determining the corresponding biofilm rheology. At the same time, there have been separate experiments

on determining the relaxation times of different biofilms [12–14]. In Table I, we summarize some of these values and the corresponding references – it becomes obvious that in most of the cases the relaxation time is of very similar order as the magical value of 18 minutes found by Shaw et al. [2].

TABLE I. Values of viscoelastic or elastic relaxation time τ_{ve} for different biofilms obtained in studies other than that of Shaw et al. [2]. The cases, for which there are multiple values of τ_{ve} for a given bacteria in a given study, are those where different strains of the same bacteria have been used.

Bacteria forming Biofilms	**Viscoelastic or elastic relaxation time τ_{ve} (minutes)**	**Reference**
Staphylococcus aureus	17.5, 18.2	Di Stefano et al. [12]
Staphylococcus epidermis	19.2	Di Stefano et al. [12]
Staphylococcus aureus	12	Rupp et. al. [13]
Staphylococcus epidermis	21.9, 21.6, 25.5	Iannitelli et al. [14]

The key hypothesis of our analysis is that the streamers, in low Reynolds number ($Re \ll 1$) background transport, form as viscous liquid jets from the biofilms. The basis of our hypothesis is that the time scale of formation of streamers t_s (t_s obtained from different experiments is in the order of several hours, see Table I in the main paper) is much larger than the viscoelastic or elastic relaxation time (τ_{ve}) of the biofilms [given the universal value of τ_{ve} of 18 minutes [2], or a value close to it (see Table I)] – consequently, the biofilms, being viscoelastic liquids, must behave as viscous liquids during the time of formation of streamers. Let us now discuss the specific cases of the biofilms, corresponding to which streamers have been observed in the experiments. The most widely studied biofilm corresponding to which streamer formation has been reported is the biofilm of the bacteria *Pseudomonas aerugionsa* [9, 15]. Shaw et al. [2] carried out experiments for the rheology of the biofilm formed from two different strains of *Pseudomonas aerugionsa* and for both of them found $\tau_{ve} \approx 18$ *minutes*. In the streamer formation (from the biofilm of the bacteria *Pseudomonas aerugionsa*) experiment of Rusconi et al. [9], the streamer formation timescale was $t_s \approx 5 - 10$ *hours*, whereas in the experiment of Drescher et al. [15] (here too the streamers are formed from the biofilm of the bacteria *Pseudomonas aerugionsa*), we get

$t_s \approx 10-20$ *hours*. Hence for the case of streamers formed from the biofilm of *Pseudomonas aerugionsa*, we clearly find $t_s \gg \tau_{ve}$. The second kind of biofilms that have been reported to disintegrate as streamers are the biofilms formed from *Pseudomonas fluorescence* [16]. Since we do not know of studies that conduct experiments to obtain the relaxation times for the biofilms obtained from this variety of bacteria, we use the idea of commonality in the viscoelastic relaxation time of the biofilms [2] and consider that the biofilms of *Pseudomonas fluorescence* will also exhibit similar viscoelastic relaxation time ($\tau_{ve} \approx 18$ *minutes*). In the experiments of Valiei et al. [16], the streamer formation (from the biofilm of the bacteria *Pseudomonas fluorescence*) timescale $t_s \approx 9$ *hours*, i.e., for this case too, we have $t_s \gg \tau_{ve}$. The third kind of biofilms from which streamer formation has been reported are the biofilms of the bacteria *Staphylococcus epidermis* [17]. Separate studies on the rheology of these biofilms [12, 13] have reported a viscoelastic relaxation time ranging from 19.2 *minutes* to 25.5 *minutes* [12, 14], i.e., values that are substantially close to the value of 18 *minutes*. In their streamer formation experiments (from biofilm of *Staphylococcus epidermis*), Weaver et al. [17] observed a streamer formation timescale $t_s \approx 6$ *hours*, i.e., here also we have $t_s \gg \tau_{ve}$. Therefore, for virtually all the experiments on streamer formation in low Reynolds transport we invariably find $t_s \gg \tau_{ve}$, establishing our hypothesis of considering the streamers (which are viscoelastic liquids) to be forming as viscous liquids. In the main paper, we have summarized in a Table (see Table I in the main paper) these values of τ_{ve} and t_s for the biofilms and the corresponding streamers, demonstrating the origin of our hypothesis. Before closing the discussion on this issue, it is worthwhile to mention here that there have been a number of studies that have modelled biofilms as viscous liquids [4, 7, 10, 18] (please note that these studies never consider or discuss streamer formation) for timescales exceeding τ_{ve}, i.e., use a hypothesis similar to that of ours.

II. SCALING OF SHEAR STRESSES AND ELASTIC STRAINS IN THE BIOFILM

The elastic strains on biofilms in presence of the flow-induced shear can be expressed as:

$$e \sim \frac{\mu_f u_c}{\ell_0 G}, \tag{1}$$

where the flow-imposed shear stress scales as $\sigma \sim \mu_f u_c/\ell_0$ (μ_f is the viscosity of the surrounding liquid, u_c is the characteristic flow velocity of the surrounding liquid and ℓ_0 is the characteristic length scale, which is typically the length scale of the flow geometry) and G is the shear modulus of the biofilm. In Table II, we discuss the possible σ and e values obtained in the streamer-formation experiments of Rusconi et al. [9, 19], Valiei et al. [16], Weaver et al [17] and Drescher et al. [15].

TABLE II. Variation of the shear stress (σ) and the strain e for different experiments on streamer formation. For all the cases we consider $\mu_f \sim 10^{-3}\ Pa-s$. Here Q is the applied flow rate.

Experiment	**Bacteria forming Biofilms**	**G (Pa)**	$Q\ (\mu L/min)$	$u_c\ (mm/s)$	$\ell_0\ (\mu m)$	$\sigma\ (Pa)$	e
Rusconi et al. [9, 19]	*Pseudomonas aeruginosa*	10 [2]	~ 1	~ 1	100	10^{-2}	10^{-3}
Valiei et al. [16]	*Pseudomonas fluorescens*	10 [2]	~ 0.2	~ 0.1	100	10^{-3}	10^{-4}
Weaver et al. [17]	*Staphylococcus epidermis*	10^3 [12]				$0.1-1$	10^{-4}– 10^{-3}
Drescher et al. [15]	*Pseudomonas aeruginosa*	10 [2]	$\sim 1-10$	$\sim 1-10$	100	$10^{-2}-10^{-1}$	10^{-3}– 10^{-2}

III. STABILITY CRITERION FOR STREAMERS AS LIQUID JETS IN COAXIAL FLOW

We consider the stability of the streamer "viscous liquid" jet, represented by a thin cylindrical jet of radius R_s and viscosity μ_b, in a background coaxial flow inside a capillary of radius ξ containing a liquid of viscosity μ_f (see Fig. 1). The stability analysis is exactly similar to that of Guillot et al.[21, 22] – therefore, we simply state the key results, without invoking detailed derivation that can be easily found in Guillot et al. [22].

The base state for the problem can be obtained by considering a steady, fully-developed pressure-driven flow (both inside and outside the jet) in the axial direction. The solution

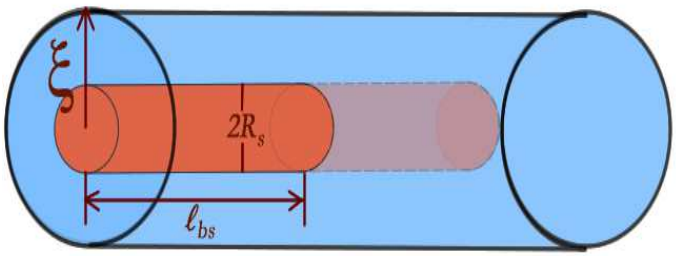

FIG. 1. Schematic of the streamer viscous jet (shown in red) in coaxial background flow. As established below, the streamer will be "absolutely" unstable breaking down into drops beyond the jet length ℓ_{bs} (breakup length).

for the base state is obtained by solving the following differential equation:

$$\begin{aligned} -\frac{dp}{dz} + \mu_b \left[\frac{1}{r}\frac{d}{dr}\left(r\frac{du}{dr}\right)\right] = 0, \quad 0 \le r \le R_s \\ -\frac{dp}{dz} + \mu_f \left[\frac{1}{r}\frac{d}{dr}\left(r\frac{du}{dr}\right)\right] = 0, \quad R_s \le r \le \xi, \end{aligned} \tag{2}$$

in presence of the boundary conditions:

$$(u)_{r=\xi} = 0, \quad \left(\mu_f \frac{du}{dr}\right)_{r=R_s^+} = \left(\mu_b \frac{du}{dr}\right)_{r=R_s^-}, \quad (u)_{r=R_s^+} = (u)_{r=R_s^-}, \quad (u)_{r=0} = \text{finite}. \tag{3}$$

to yield:

$$\begin{aligned} u = -\frac{1}{4\mu_b}\frac{dp}{dz}\left[\left(R_s^2 - r^2\right) - \frac{\mu_b}{\mu_f}\left(\xi^2 - R_s^2\right)\right] \ (0 \le r \le R_s) \\ u = -\frac{1}{4\mu_f}\frac{dp}{dz}\left(\xi^2 - r^2\right) \ (R_s \le r \le \xi). \end{aligned} \tag{4}$$

With this base state, one can perform a perturbation analysis to obtain the following criterion for the stability of the jet (for detail derivation, please refer to Guillot et al. [22]):

$$Ka = \frac{C_1 F\left(\frac{R_s}{\xi}, \frac{\mu_b}{\mu_f}\right)}{\left(\frac{R_s}{\xi}\right)^3 E\left(\frac{R_s}{\xi}, \frac{\mu_b}{\mu_f}\right)}, \tag{5}$$

where $C_1 = \frac{5+\sqrt{7}}{18}\sqrt{\frac{24}{\sqrt{7}-1}}$, Ka is capillary number at the scale of the capillary, expressed as $Ka = (-\partial p/\partial z)\xi^2/\gamma = \mu_f u_c/\gamma$ and E and F are functions expressed as:

$$E\left(\frac{R_s}{\xi}, \frac{\mu_b}{\mu_f}\right) = -4\left(\frac{R_s}{\xi}\right) + \left(8 - \frac{4\mu_f}{\mu_b}\right)\left(\frac{R_s}{\xi}\right)^3 + 4\left(\frac{\mu_f}{\mu_b} - 1\right)\left(\frac{R_s}{\xi}\right)^5, \tag{6}$$

$$F\left(\frac{R_s}{\xi},\frac{\mu_b}{\mu_f}\right)=\left[4-\frac{\mu_f}{\mu_b}+4\ln\left(\frac{R_s}{\xi}\right)\right]\left(\frac{R_s}{\xi}\right)^4+\left(-8+\frac{4\mu_f}{\mu_b}\right)\left(\frac{R_s}{\xi}\right)^6+\left[4-\frac{3\mu_f}{\mu_b}-4\left(1-\frac{\mu_f}{\mu_b}\right)\ln\left(\frac{R_s}{\xi}\right)\right.$$

This stability criterion [eq.(5)] is plotted in Fig. 2 in the main paper. In the same figure, we plot the experimental conditions (employed in streamer formation experiments), represented by the corresponding Ka and R_s/ξ values (Table II in the main paper summarizes the Ka values witnessed in the different experiments). Now the experiments are typically performed in square [9, 15] or rectangular [16] geometries. Important to note that in these geometries (with characteristic dimension h), $Ka=-(\partial p/\partial z)(h/2)^2/\gamma=\mu_f u_c/\gamma$ (i.e., the definition of Ka remains same as that in a circular capillary; here γ is the surface tension between the streamer liquid and the bulk liquid) and R_s/ξ is replaced by $R_s/(h/2)$ (i.e., it still remains the ratio of the jet radius to the characteristic dimension of the flow geometry). What changes, however, is the equation for the stability criterion [eq.(5)]. But, as has been clearly demonstrated in Guillot et al. [22], such a change is only important for substantially large (> 0.3) values of R_s/ξ or $R_s/(h/2)$. However, we always find that $R_s \ll \xi$ or $R_s \ll h/2$. Therefore, we can safely assume that the stability plots remain unchanged with the change in geometry. Hence it is perfectly valid to plot the experimental conditions, represented by Ka and R_s/ξ values, for streamer formation experiments in square or rectangular geometries, in the instability plot for the circular capillaries.

IV. ESTIMATION OF THE BREAKUP LENGTH OF THE STREAMER VISCOUS JET IN COAXIAL FLOW

Considering the background flow to be coaxial with the streamer viscous jet, we can pinpoint that the streamer jet experiences an "absolute instability" (see previous section) triggering a spontaneous breakdown of the jet into drops. Like any jet breakup, here too, we can quantify the breakup by the corresponding "breakup length" ℓ_{bs}. This length is specially significant for the set of microscale experiments (with system length scale ℓ_0) [9, 15, 16] that report the formation of streamers. In case $\ell_{bs} > \ell_0$, the streamers continue as unbroken viscous jets attached to point from where they originated (e.g., microposts in the experiment of Valiei et al. [16]). In this section, we shall provide a scaling estimate of ℓ_{bs} with the background flow being coaxial with the streamer viscous jet. Following Javadi

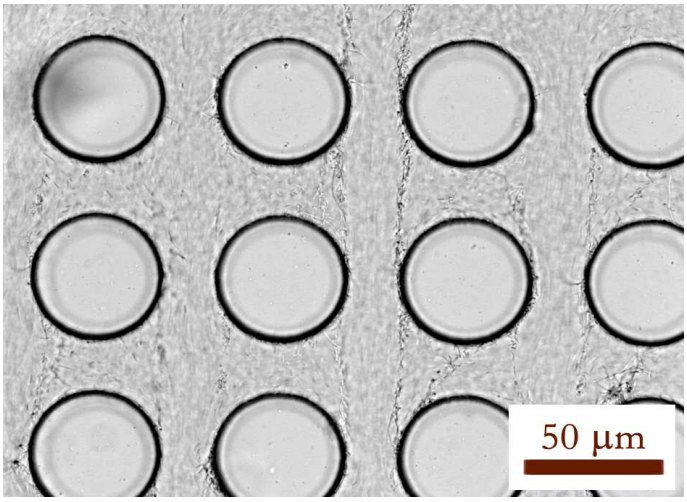

FIG. 2. A continuous streamer formation between two successive cylindrical micro-posts. Fluid flow is from top to bottom. Reproduced from Valiei et al. [16] by permission of The Royal Society of Chemistry.

et al. [23], which estimates the breakup length for the falling viscous jets, we start with the equations governing the one dimensional [plug flow, represented by the uniform velocity $v(z,t)$] of high viscous slender liquid jets:

$$\frac{\partial A}{\partial t} + \frac{\partial}{\partial z}(Av) = 0, \tag{8}$$

$$\rho A\left(\frac{\partial v}{\partial t} + v\frac{\partial v}{\partial z}\right) = 3\mu_b \frac{\partial}{\partial z}\left(A\frac{\partial v}{\partial z}\right) - \gamma A\frac{\partial \kappa}{\partial z} + f_0, \tag{9}$$

$$\kappa = \frac{1}{R_s\sqrt{1+\left(\frac{dR_s}{dz}\right)^2}} - \frac{\frac{d^2R_s}{dz^2}}{\left[1+\left(\frac{dR_s}{dz}\right)^2\right]^{3/2}}, \tag{10}$$

where ρ is the density of the viscous jet, $R_s(z,t)$ is the radius of the jet, $A = \pi R_s^2$, κ is the mean curvature and f_0 is the externally imposed force (per unit length) on the fluid. For a falling jet this external force is due to gravity, so that $f_0 = \rho g A$ (g is the acceleration due to gravity), whereas for our case it is the external shear imposed by the background flow, i.e., $f_0 \sim 2\pi R_s \mu_f u_c/\ell_0$. We now invoke an analysis similar to Javadi et al. [23]. For a steady state of the jet, if we neglect the surface tension ($\gamma = 0$), the momentum balance will read:

$$\rho A v\frac{\partial v}{\partial z} = 3\mu_b \frac{\partial}{\partial z}\left(A\frac{\partial v}{\partial z}\right) + f_0 \tag{11}$$

For smaller jet length ($z \sim \ell_j$, ℓ_j is the jet length), viscous forces are more dominant than the inertial forces, and therefore f_0 is balanced by viscous forces for $\ell_j < \ell_c$ and f_0 is balanced

by the inertial forces for $\ell_j > \ell_c$ (here ℓ_c denotes the critical jet length where the viscous and the inertial forces balance each other). This is exactly equivalent to the case studied by Javadi et al. [23], where the weight of the jet (equivalent to f_0) is balanced by the viscous forces for smaller jet lengths and inertial forces for larger jet lengths. This transition length (ℓ_c) can thus be quantified by equating the viscous forces with the inertial forces, which yield:

$$\ell_c \sim \frac{\mu_b}{\rho u_c}. \tag{12}$$

For the experiments studying the streamer formation, $u_\infty \sim 10^{-4} - 10^{-2}\ m/s$ [9, 15, 16], $\mu_b \sim 10^4\ Pa - s$ [15, 16] and $\rho \sim 10^3\ kg/m^3$ [24, 25], we get $\ell_c \sim 10^4 - 10^6\ m$, i.e., $\ell_c \gg \ell_0$. Hence the streamer jet is always driven by the balance of the viscous force and the applied force f_0. Consequently, we can write the velocity of the jet at a given z as [using eq.(11) to obtain the change in velocity Δu]:

$$u \sim u_c + \Delta u \sim u_c \left(1 + \frac{2\mu_f}{\mu_b}\frac{z^2}{r\ell_0}\right). \tag{13}$$

Using $z \sim \ell_0$, $\mu_f/\mu_b \sim 10^{-7}$ and $\ell_0/r \sim 10^2$, we get:

$$u \sim u_c, \tag{14}$$

i.e., the extremely large viscosity of the streamer ensures that its average velocity remains close to the bulk value.

One needs to account for the surface tension effects when one needs to pinpoint the stability of the jet – the surface tension tries to breakdown the jet and the viscosity resists this effect. Consequently, following Javadi et al. [23] and Eggers and Dupont [26], we get the perturbation growth rate (for the high viscosity limit) Γ_p as:

$$\Gamma_p \sim \frac{\gamma}{\mu_b R_s}. \tag{15}$$

On the other hand, the characteristic time scale for the streamer jet can be quantified as z_0/u_c (where z_0 is the characteristic length scale for the jet). Following Javadi et al. [23], we quantify that the breakup occurs at the distance $z_0 \equiv \ell_{bs}$ where the Rayleigh growth time (quantified as Γ_p^{-1}) becomes smaller than the characteristic time for the jet motion ($z_0/u_c = \ell_{bs}/u_c$), and hence:

$$\frac{\ell_{bs}}{R_s} \sim \frac{\mu_b u_c}{\gamma}. \tag{16}$$

Please note that like the case of inviscid flow, here too the breakup gets delayed if the velocity is large (off course for the inviscid case where inertia resists the surface tension mediated breakup, ℓ_{bs} demonstrates a different scaling with u). Using eq.(16) we can estimate the breakup length for the streamer viscous jets for different experiments. For example, for Valiei et al. [16], we get $\ell_{bs} \sim 100\ \mu m$ (using $R_s \sim 1\ \mu m$, $\mu_b \sim 10^4\ Pa-s$, $\gamma \sim 0.01\ N/m$ and $u_c \sim 10^{-4}\ m/s$), whereas for Drescher et al. [15], we get $\ell_{bs} \sim 1-10\ mm$ (using $u_c \sim 10^{-3}-10^{-2}\ m/s$ and all other parameters identical as above). In Valiei et al. [16], we indeed find that the streamers continue as long unbroken jets/filaments (see Fig. 2).

V. ESTIMATION OF THE BREAKUP LENGTH OF THE STREAMER VISCOUS JET IN CROSSFLOW

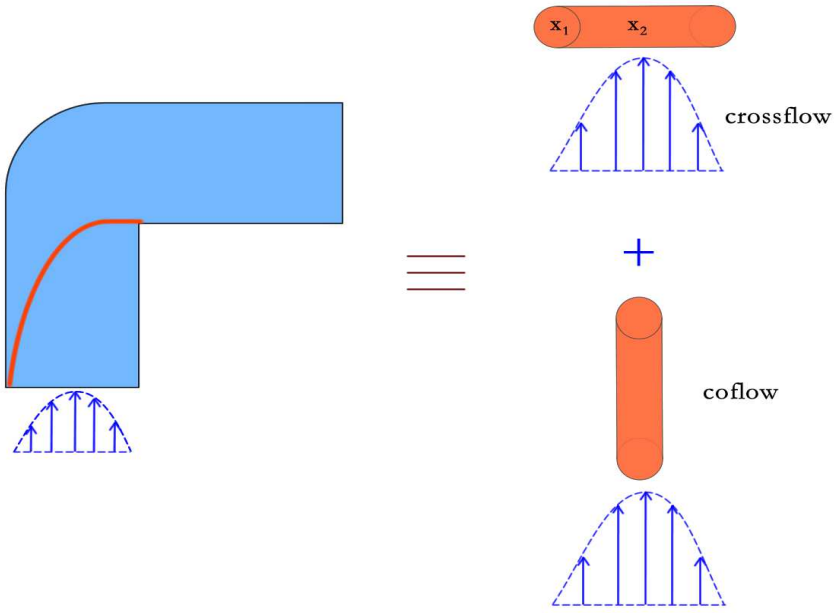

FIG. 3. Schematic illustrating the manner in which the streamers are partly in crossflow in the experiments of Rusconi et al. [9] and Drescher et al. [15]. The momentum of this crossflow (necessary to breakup the streamer liquid jet) is least at the point x_1 (at the wall) and maximum at the point x_2 (at the channel center).

Here we shall provide an analysis to calculate the breakup length for the streamer jet in case it is entirely in a crossflow (see Fig. 3 for the schematic explanation). A jet in a crossflow is characterized by different vortical features as has been extensively described

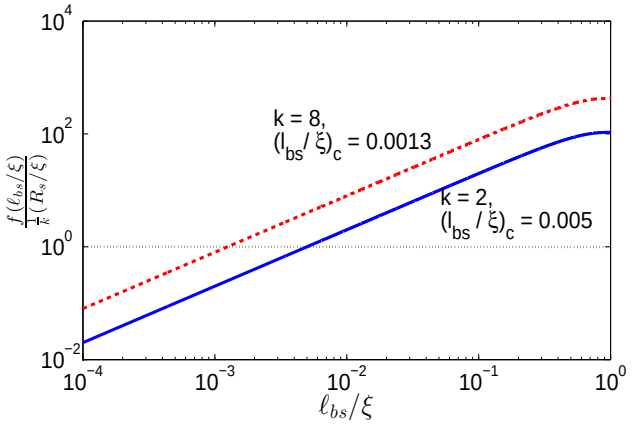

FIG. 4. (Color Online) Variation of $\frac{f(\ell_{bs}/\xi)}{(1/k)(R_s/\xi)}$ [where $f(\ell_{bs}/\xi) = \frac{\ell_{bs}}{\xi} - \frac{2}{3}\left(\frac{\ell_{bs}}{\xi}\right)^3 + \frac{1}{5}\left(\frac{\ell_{bs}}{\xi}\right)^5$] with ℓ_{bs}/ξ for different values of k. This plot provides solution to eq.(18) – the solution yields $(\ell_{bs}/\xi)_c$ and ensures that $\frac{f(\ell_{bs}/\xi)}{(1/k)(R_s/\xi)} = 1$ (denoted with a dotted line).

in several literature [27]. The most relevant characterization of the jet in a crossflow is to quantify the trajectory (x, y) of the jet as a function of the ratio of the momentum of jet to that of the crossflow [28]. We quantify the breakup length of a jet in a crossflow as the distance from the point of origin of the jet, corresponding to which the inertial momentum of the crossflow gets balanced by the momentum of the jet. This distance is also the distance over which the jet gets deflected from its path. This idea can be understood in the present context as well. The momentum of the cross flow is very small close to the wall, so that the jet continues unbroken at such locations; however towards the centre of the crossflow, where its momentum increases, the momentum of the jet and the crossflow balances each other and there can be deflection and breakup of the jet (see Fig. 3). Following Muppidi and Mahesh [28], we can obtain this breakup length (or the deflection distance ℓ_{bs}) as:

$$\rho_{cf}\pi 2R_s \int_0^{\ell_{bs}} u_{cf}^2 dr = \rho_j \int_A u_j^2 dA \tag{17}$$

where u_{cf}, ρ_{cf} and u_j, ρ_j are the velocities and densities of the background flow and the jet, respectively. Using $u_{cf} = 2u_{av}\left(1 - r^2/\xi^2\right) = u_{max}\left(1 - r^2/\xi^2\right)$ (here u_{av} and u_{max} are the average and the maximum velocities), $\rho_{cf} \approx \rho_j$ [24, 25] and $A = \pi R_s^2$, we get:

$$\frac{\ell_{bs}}{\xi} - \frac{2}{3}\left(\frac{\ell_{bs}}{\xi}\right)^3 + \frac{1}{5}\left(\frac{\ell_{bs}}{\xi}\right)^5 = \frac{1}{k}\frac{R_s}{\xi}, \tag{18}$$

where $k = 8$ for $u_j = u_{av}$ and $k = 2$ for $u_j = u_{max}$. In Fig. 4, we plot the variation of $\frac{f(\ell_{bs}/\xi)}{(1/k)(R_s/\xi)}$ [where $f(\ell_{bs}/\xi) = \frac{\ell_{bs}}{\xi} - \frac{2}{3}\left(\frac{\ell_{bs}}{\xi}\right)^3 + \frac{1}{5}\left(\frac{\ell_{bs}}{\xi}\right)^5$] with ℓ_{bs}/ξ and from there we get the

solution of eq.(18), i.e., the real values of ℓ_{bs}/ξ [we call them $(\ell_{bs}/\xi)_c$] that satisfy eq.(18). From the solutions, we can see that deflection heights (or breakup lengths) for the streamer jet in crossflow is extremely small: e.g., $(\ell_{bs}/R_s)_{k=2} = 0.5$ and $(\ell_{bs}/R_s)_{k=8} = 0.13$. This implies that if the jet is in crossflow the breakup will start to occur almost instantaneously after the jet starts. Therefore even when there is slight component of crossflow in the dynamics of a given streamer jet – e.g., in the experiments of Rusconi et al. [9] and Drescher et al. [15] the streamer is not aligned along the flow direction and therefore will experience some contribution of the crossflow – the streamer will start to breakdown into drops spontaneously and the corresponding breakup length will be substantially smaller than that predicted in eq.(16).

Please note for streamers, either in coaxial flow or crossflow, there may be a possible variation in the jet breakup length due to the addition of mass (such mass addition alters the instability dynamics [29, 30]). However, for co-axial flow [16], the rate of mass addition $dR_s/dt = \beta C A_{ac} D/4 \sim 10^{-11}\ m/s$, (see section VI for the meaning of the different symbols) i.e., it is much smaller than the average velocity of the streamers ($\sim u_c \sim 10^{-4}\ m/s$) and hence we neglect the effect of mass addition in variation of the breakup length ℓ_{bs} for the coaxial flow [16]. However, the rate of mass addition in crossflow [9, 15], will be substantially higher and would cause an even further reduction in the breakup length [29, 30]. We refrain from that analysis, since that would only establish our present hypothesis without providing any new insight.

VI. TIME VARIATION OF GROWTH OF BIOFILM STREAMERS

Drescher et al. [15] provided a detailed derivation of the growth rate of the radius of the biofilm streamers. They explained that such growth occurs due to the adsorption of advected bacteria that adds mass to the biofilm streamers. Representing the biofilm streamers as a "solid" object of a given radius R_s, with its axis oriented transverse to the flow direction, the authors established that for the non-porous "solid" streamers, $R_s(t) \sim t^{3/4}$, whereas for a completely transparent (extreme case of a porous) streamer, $R_s(t) \sim \exp(t/\tau_{theory})$, where τ_{theory} is the time scale for the growth of the streamers. Experiments suggested a very rapid growth rate of the streamers, which could only be explained by such exponential dependence of R_s on time. It was further shown that $\tau_{theory} \sim 1/(Cu_c)$, where C is the

cell concentration in the bulk and u_c is the characteristic velocity (which is the average flow speed in the microchannel). From experiments, they recovered $1/u_c$ and $1/C^{0.6}$ variations of τ_{theory}, i.e., there was a quantitative match of velocity dependence and a pretty agreeable qualitative match of concentration dependence. Here we shall first show that there is an error in Drescher et al.'s derivation of the $R_s(t) \sim \exp(t/\tau_{theory})$; on being corrected such exponential dependence no longer exists. The starting point of the equation that leads to $R_s(t) \sim \exp(t/\tau_{theory})$ is that the streamer cross sectional area (πR_s^2) increases when a cell is caught by the streamer that adds an area A_{ac} to the streamer cross section. Therefore,

$$2\pi R_s \frac{dR_s}{dt} = \beta I A_{ac}, \tag{19}$$

where I is the number of cells per unit length of the streamer per unit time and β is the fraction of cells that get caught in the streamer. Drescher et al. [15] expressed $I = 2R_s J = 2R_s CV$ (where J is the flux of the cells and V is the velocity of cell migration through the streamer), so that eq.(19) reduces to:

$$\pi \frac{dR_s}{dt} = \beta C V A_{ac}, \tag{20}$$

We now discuss the fundamental errors in eq.(20). First and foremost the units on the two sides of eq.(20) do not match. The unit on LHS is m/s, whereas that in RHS (considering the units of C, V and A_{ac} as $1/m^3$ [15], m/s and m^2, respectively) is $1/s$. Just to ensure that there is a match in the dimensions, Drescher et al. [15] used a unit of μm^3 (i.e., unit of volume) for A_{ac}. The second and more non-intuitive issue concerns the balance law expressed in eq.(19). The cells get added to the streamer and contribute to an increase in the streamer surface area, with the streamer being in cross flow. Therefore, the area that changes is not the cross sectional area, rather it is surface area of the cylindrical streamer, expressed as $A_s = 2\pi R_s \ell_s$ (where ℓ_s is the length of the streamers). Also this rate change of area must be equal to the area change caused by total number of cells per unit time that get adsorbed (and contributes to an area change) of the streamers. Therefore, we can write:

$$\frac{d}{dt}(A_s) = \beta(Flux \times A_s)A_{ac} \Rightarrow \frac{dR_s}{dt} = \beta C V R_s A_{ac}. \tag{21}$$

One can clearly see that RHS and LHS of eq.(21) have same units (m/s). Using $V \approx R_s \Delta p/7\mu_f$ (where Δp is the pressure drop along the streamer; see Drescher et al. [15] for the derivation of this expression of V), we can re-write eq.(21) as:

$$\frac{dR_s}{dt} = \frac{\beta C \Delta p A_{ac}}{7\mu_f} R_s^2. \tag{22}$$

Integrating eq.(22) in presence of the condition $R_s(t=0) = R_{s,0}$, we shall get:

$$\frac{R_s}{R_{s,0}} = \frac{1}{1 - t/\tau_{theory,1}}, \tag{23}$$

where

$$\tau_{theory,1} = \frac{7\mu_f}{\beta C \Delta p A_{ac} R_{s,0}} \tag{24}$$

is the time scale for streamer formation. Also from eq.(23), we can state that on considering a "solid" streamer, we shall never get an exponential increase in the streamer thickness (as has been observed in experiments [15]). Please note, however, that using $u_c \propto \Delta p/\mu_f$, we do get $\tau_{theory,1} \propto 1/(Cu_c)$ from eq.(24).

We now consider the increase in the area of the "viscous liquid" streamers, as considered in the present case. We have discussed previously that on account of geometry-induced crossflow, the streamer liquid jet may break down into smaller droplets [9, 15] of radius approximately equal to R_s. Therefore, we are now considering the area enhancement (on account of advective influx of bacteria) of spherical liquid drops (of area $4\pi R_s^2$). Therefore, following the same principle of area increase as the case of Drescher et al. [15], we may write:

$$\frac{d}{dt}(4\pi R_s^2) = 4\pi\beta C V R_s^2 A_{ac}, \tag{25}$$

so that using $V \approx u_c$ (this approximation stems from the fact that being a "liquid" drop, the streamer does not induce a major variation in the magnitude of cross flow velocity; such variation is typically triggered by a solid object on account of "no slip" and "no penetration" boundary condition at its surface), we can write:

$$\frac{dR_s}{dt} = \frac{\beta C u_c A_{ac}}{2} R_s, \tag{26}$$

which on integration [with $R_s(t=0) = R_{s,0}$] yields:

$$\frac{R_s}{R_{s,0}} = \exp\left(t/\tau_{theory,2}\right), \tag{27}$$

where

$$\tau_{theroy,2} = \frac{2}{\beta C u_c A_{ac}}. \tag{28}$$

Please note that such exponential behaviour (having a time constant different from $\tau_{theory,2}$) can also be predicted by assuming the streamers to be unbroken long cylindrical liquid jets (with constant length) – problem with such an assumption is that it violates the stability condition, which forbids the streamers to sustain as long unbroken jets in cross flows.

Therefore, we conclude that only by considering a "viscous liquid" state of the streamers that breakdown into droplets in presence of flow-geometry-induced crossflow, we can explain such exponential growth of streamer surface area.

It is worthwhile to discuss here the manner in which streamer growth rate may vary if one considers a purely diffusion-mediated transport of the "area-enhancing" cells to the "viscous liquid" streamer jets. This typically occurs if the streamer jet is unbroken and is coaxial with the background flow, as in Valiei et al. [16]. In this case, $V \approx V_D$, where V_D is the diffusion velocity expressed as $V_D = d\ell_D/dt = D/(2\ell_D)$ (where D is the diffusivity and ℓ_D is the diffusion length scale for the cell migration into the streamers). With $\ell_D \approx R_s$ and using $V \approx V_D$ in eq.(21), we shall get:

$$\frac{dR_s}{dt} = \frac{\beta C A_{ac} D}{2}, \tag{29}$$

which on integration [with $R_s(t=0) = R_{s,0}$] yields:

$$\frac{R_s}{R_{s,0}} = 1 + \frac{t}{\tau_{theory,3}} \tag{30}$$

where

$$\tau_{theroy,3} = \frac{2R_{s,0}}{\beta C A_{ac} D}. \tag{31}$$

We can also obtain a ratio of these different time scales, such as:

$$\frac{\tau_{theory,1}}{\tau_{theory,2}} \approx \frac{7}{2}\frac{L_t^2}{L_a R_{s,0}}, \tag{32}$$

and

$$\frac{\tau_{theory,3}}{\tau_{theory,2}} \approx \frac{R_{s,0} u_c}{D}. \tag{33}$$

To obtain eq.(32), we used $u_c \approx (1/\mu_f)(\Delta p/L_a)L_t^2$ (where L_t is the transverse dimension of the channel and L_a is the axial length over which the pressure drop occurs). From the experiment of Drescher et al. [15] or Rusconi et al. [9, 19], we get $L_t \approx L_a$, but $R_{s,0} \ll L_t$, implying $\tau_{theory,1} \gg \tau_{theory,2}$. Also using $D \approx 10^{-10} m^2/s$, $R_{s,0} \approx 1 - 10\ \mu m$ and $u_c \sim 10^{-3}\ m/s$, we get from eq.(33), $\tau_{theory,3} \gg \tau_{theory,2}$. Therefore, we establish that considering streamers as liquid jets that break down spontaneously into drops (on account of flow-geometry-induced crossflow), we not only get an exponential increase in the streamer thickness (which is not possible with "solid" state streamer), but also get a time scale that is independent of initial streamer thickness and is substantially smaller (indicating much faster clogging effect) than the time scale corresponding to the case of "solid" streamer or the case of diffusive transport.

VII. REDUCTION IN BULK FLOW RATE DUE TO PRESENCE AND BREAKDOWN OF "LIQUID" STREAMER

FIG. 5. Schematic illustrating the manner in which the streamers disintegrated due to crossflow may block the flow passage causing the catastrophic "clogging" effect[15]. The cylindrical streamer jet will breakdown into spheres; however, we provide a simplistic estimate of flow reduction considering them to cylinders aligned with the flow direction.

In this section, we shall discuss two issues related to the role of streamers in causing reduction in the flow rate – such reduction signifies the role of the streamers in "clogging" the flow. First, we shall show that streamers as cylindrical "viscous liquid" jets, placed in the middle of the flow passage can lead to a substantial reduction in the flow rate. This reduction, depending on the ratio of the streamer thickness to the channel dimension, may be more significant than the reduction caused by the "solid" state streamer placed in the middle of the flow passage [15]. Second, we demonstrate that the breakdown of the "viscous liquid" streamer jet into droplets (on account of presence of geometry-mediated crossflow) may substantially augment this reduction (see Fig. 5 for the schematic).

We start by considering the flow rate for a steady pressure-driven fully developed flow inside a cylindrical capillary of radius ξ, which can be expressed as:

$$Q_0 = -\frac{\pi}{8\mu_f}\frac{dp}{dz}\xi^4, \tag{34}$$

where $-dp/dz$ is the applied pressure gradient. Following Drescher et al. [15], for a wall attached biofilm of thickness $\epsilon\xi$ ($\epsilon \ll 1$), which leads to a reduced radius of $\xi - \epsilon\xi$, we get the flow rate as Q_{film} as:

$$Q_{film} = -\frac{\pi}{8\mu_f}\frac{dp}{dz}\left(\xi - \epsilon\xi\right)^4, \tag{35}$$

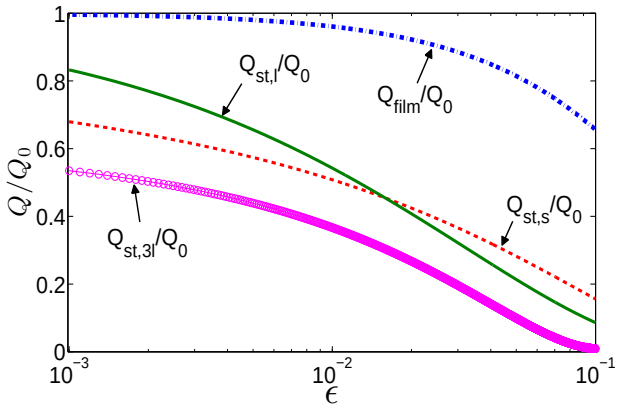

FIG. 6. (Color Online) Variation of the dimensionless flow rate with ϵ (dimensionless thickness of the wall-attached biofilm) for four different cases, namely with wall-attached biofilm (Q_{film}/Q_0), with "solid" streamer placed along the center of the cylindrical capillary ($Q_{st,s}/Q_0$), with "liquid" streamer placed along the center of the cylindrical capillary ($Q_{st,l}/Q_0$), with three liquid streamers placed symmetrically along the capillary cross section ($Q_{st,3l}/Q_0$).

so that

$$\frac{Q_{film}}{Q_0} = (1-\epsilon)^4\,, \tag{36}$$

indicating a reduction in the flow rate. Drescher et al. [15] argued that if a long cylindrical "solid" streamer, having the same mass as the wall-attached biofilm, is placed inside the middle of the capillary, it will lead to a substantially larger reduction in the flow rate. Considering the radius of this "solid" cylindrical streamer to be R_s, and assuming that this streamer is placed along the centerline of the channel, providing a no-slip surface, Drescher et al. [15] showed that the corresponding flow rate $Q_{st,s}$ is:

$$\frac{Q_{st,s}}{Q_0} = \frac{\left(\frac{R_s}{\xi}\right)^4\left[1-\ln\left(\frac{R_s}{\xi}\right)\right]+1+\ln\left(\frac{R_s}{\xi}\right)-2\left(\frac{R_s}{\xi}\right)^2}{\ln\left(\frac{R_s}{\xi}\right)}. \tag{37}$$

In case the streamers are "viscous liquid" jets placed in the middle of the capillary, we get the velocity field u inside ($0 \le r \le R_s$) and outside ($R_s \le r \le \xi$) the streamers as expressed in eq.(4). Hence the new flow rate in the bulk $Q_{st,l}$ (excluding the streamers) can be expressed as:

$$\frac{Q_{st,l}}{Q_0} = \frac{\int_{R_s}^{\xi} 2\pi r u dr}{Q_0} = \left(1-\frac{R_s}{\xi}\right)^4, \tag{38}$$

From the volume conservation, we can relate ϵ and R_s as:

$$\frac{R_s}{\xi} = \left(2\epsilon + \epsilon^2\right)^{1/2}, \tag{39}$$

so that we can express eqs.(37,38) solely in terms of ϵ. Variation in the flow rates for different conditions is depicted in Fig. 6. We can clearly see that depending on ϵ, we get a reduced flow rate for "liquid" state streamer jets.

"Liquid" jet streamers will break down into smaller segments on account of presence of geometry-mediated crossflow [9, 15] (see above). Also since crossflow is the primary breaking mechanism for the streamers, this will mean that the broken smaller segments (of the streamers) will be located transverse to the flow. A simple analogy can be 3 streamer segments (of identical radius as the single streamer) placed symmetrically along the transverse direction, i.e., at the following three locations: $(-\xi/2 - R_s) \leq r \leq (-\xi/2 + R_s)$, $-R_s \leq r \leq R_s$ and $(\xi/2 - R_s) \leq r \leq (\xi/2 + R_s)$ (see Fig. 5). Please note that instead of considering drops, we consider cylindrical segments of the broken streamer – this is not strictly correct, since the streamer jet will breakdown into drops. However, change of such geometry of the broken segments will only change the flow field (induce a transverse component of the flow field) at a given cross-section, but this will not change the overall flow reduction, since that reduction depends only on the axial flow, which will not be substantially affected. For such a case (see Fig. 5) the governing equation would be:

$$\begin{aligned}
-\frac{dp}{dz} + \mu_b \left[\frac{1}{r}\frac{d}{dr}\left(r\frac{du}{dr}\right)\right] = 0, \quad 0 \leq r \leq R_s, \\
-\frac{dp}{dz} + \mu_f \left[\frac{1}{r}\frac{d}{dr}\left(r\frac{du}{dr}\right)\right] = 0, \quad R_s \leq r \leq (\xi/2 - R_s), \\
-\frac{dp}{dz} + \mu_b \left[\frac{1}{r}\frac{d}{dr}\left(r\frac{du}{dr}\right)\right] = 0, \quad (\xi/2 - R_s) \leq r \leq (\xi/2 + R_s), \\
-\frac{dp}{dz} + \mu_f \left[\frac{1}{r}\frac{d}{dr}\left(r\frac{du}{dr}\right)\right] = 0, \quad (\xi/2 + R_s) \leq r \leq \xi.
\end{aligned} \tag{40}$$

and the corresponding boundary conditions are

$$\begin{aligned}
&(u)_{r=\xi} = 0, \quad \left(\mu_f \frac{du}{dr}\right)_{r=(\xi/2+R_s)^+} = \left(\mu_b \frac{du}{dr}\right)_{r=(\xi/2+R_s)^-}, \quad (u)_{r=(\xi/2+R_s)^+} = (u)_{r=(\xi/2+R_s)^-}, \\
&\left(\mu_b \frac{du}{dr}\right)_{r=(\xi/2-R_s)^+} = \left(\mu_f \frac{du}{dr}\right)_{r=(\xi/2-R_s)^-}, \quad (u)_{r=(\xi/2-R_s)^+} = (u)_{r=(\xi/2-R_s)^-}, \\
&\left(\mu_f \frac{du}{dr}\right)_{r=R_s^+} = \left(\mu_b \frac{du}{dr}\right)_{r=R_s^-}, \quad (u)_{r=R_s^+} = (u)_{r=R_s^-}, \quad (u)_{r=0} = \text{finite}.
\end{aligned} \tag{41}$$

The solution for the flow fields are:

$$u = -\frac{1}{4\mu_b}\frac{dp}{dz}\left[\left(2\xi R_s + R_s^2 - r^2\right) + \frac{\mu_b}{\mu_f}\left(\xi^2/2 - R_s^2\right)\right] \ [0 \le r \le R_s],$$
$$u = -\frac{1}{4\mu_f}\frac{dp}{dz}\left[\left(\xi^2/2 - 2R_s^2 - r^2\right) + 2\frac{\mu_f}{\mu_b}\xi R_s\right] \ [R_s \le r \le (\xi/2 - R_s)],$$
$$u = -\frac{1}{4\mu_b}\frac{dp}{dz}\left[\left((\xi/2 + R_s)^2 - r^2\right) + \frac{\mu_b}{\mu_f}\left(\xi^2 - (\xi/2 + R_s)^2\right)\right] \ [(\xi/2 - R_s) \le r \le (\xi/2 + R_s)],$$
$$u = -\frac{1}{4\mu_f}\frac{dp}{dz}\left(\xi^2 - r^2\right) \ [(\xi/2 + R_s) \le r \le \xi]. \tag{42}$$

The resulting flow rate in the bulk $Q_{st,3l}$ (excluding the streamers) can be expressed in dimensionless form as:

$$\frac{Q_{st,3l}}{Q_0} = \frac{\int_{R_s}^{\xi/2-R_s} 2\pi r u dr + \int_{\xi/2+R_s}^{R_s} 2\pi r u dr}{Q_0} =$$
$$1 - \left(\frac{1}{2} + \frac{R_s}{\xi}\right)^2\left[2 - \left(\frac{1}{2} + \frac{R_s}{\xi}\right)^2\right] + \left[1 - 4\left(\frac{R_s}{\xi}\right)^2 + 4\frac{\mu_f}{\mu_b}\frac{R_s}{\xi}\right]\left(\frac{1}{4} - \frac{R_s}{\xi}\right) - \left(\frac{1}{2} - \frac{R_s}{\xi}\right)^4 + \left(\frac{R_s}{\xi}\right)^4, \tag{43}$$

and we get the dimensionless flow rate $Q_{st,3l}/Q_0$ in terms of ϵ using eq.(39). The result is plotted in Fig. 6, and we clearly find a substantially reduced flow rate, as compared to the "solid" streamer, for the entire spectrum of ϵ.

---

[1] I. Klapper et al., Biotechnol. Bioeng. **80**, 289 (2002).

[2] T. Shaw et al., Phys. Rev. Lett. **93**, 098102 (2004).

[3] P. Stoodley et al., J. Ind. Microbiol. Biotechnol. **29**, 361 (2002).

[4] H. F. Winstanley et al., Proc. Roy. Soc. A **467**, 1449 (2011).

[5] B. W. Towler et al., Biofouling **19**, 279 (2003).

[6] A. K. Epstein et al., New J. Phys. **15**, 095018 (2013).

[7] I. Klapper, Bull. Math. Biol. **74**, 2917 (2012).

[8] M. Fauvart, Soft Matter **8**, 70 (2012).

[9] R. Rusconi et al., Biophys. J. **100**, 1392 (2011).

[10] T. Zhang and I. Klapper, Water Sci. Technol. **61**, 2957 (2010).

[11] I. Klapper and J. Dockery, Phys. Rev. E **74**, 031902 (2006).

[12] A. Di Stefano et al., Microb. Biotechnol. **2**, 634 (2009).

[13] C. J. Rupp et al., Appl. Environment. Microbiol. **71**, 2175 (2005).

[14] A. Iannitelli, Int. J. Mol. Sci. **12**, 5039 (2011).

[15] K. Drescher et al., Proc. Nat. Acad. Sci. USA **110**, 4345 (2013).

[16] A. Valiei et al., Lab Chip **12**, 5133 (2012).

[17] W. M. Weaver et al., Appl. Environment. Microbiol. **78**, 5890 (2012).

[18] T. Zhang, Bull. Math. Biol. **74**, 1427 (2012).

[19] R. Rusconi et al., J. Roy. Soc. Interface **7**, 1293 (2010).

[20] J. Eggers, Phys. Rev. Lett. **71**, 3458 (1993).

[21] P. Guillot et al., Phys. Rev. Lett. **99**, 104502 (2007).

[22] P. Guillot, A. Colin, and A. Ajdari, Phys. Rev. E **78**, 016307 (2008).

[23] A. Javadi et al., Phys. Rev. Lett. **110**, 144501 (2013).

[24] K. Azetsu-Scott and U. Passow, Limnol. Oceanogr. **49**, 741 (2004).

[25] S. Skraber et al., Biofilms **2**, 105 (2005).

[26] J. Eggers and T. F. Dupont, J. Fluid Mech. **262**, 205 (1994).

[27] A. Karagozian, Prog. Energy Combust. Sci. **30**, 1 (2010).

[28] S. Muppidi and K. Mahesh, J. Fluid Mech. **530**, 81 (2005).

[29] H. C. Burkholder and J. C. Berg, AIChE J. **20**, 863 (1974).

[30] G. O. Collantes, E. Yariv, and I. Frankel, J. Fluid Mech. **474**, 95 (2003).